Journal of Volcanology and Geothermal Research 272 (2014) 16–22

Contents lists available at ScienceDirect

Journal of Volcanology and Geothermal Research

journal homepage: www.elsevier.com/locate/jvolgeores

Permeability measurements of Campi Flegrei pyroclastic products: An example from the Campanian Ignimbrite and Monte Nuovo eruptions

M. Polacci [a,*], C. Bouvet de Maisonneuve [b], D. Giordano [c], M. Piochi [d], L. Mancini [e], W. Degruyter [f], O. Bachmann [g]

[a] Istituto Nazionale di Geofisica e Vulcanologia, Sezione di Pisa, Pisa, Italy
[b] Earth Observatory of Singapore, Nanyang Technological University, Singapore
[c] Dipartimento di Scienze della Terra, Università degli Studi di Torino, Torino, Italy
[d] Istituto Nazionale di Geofisica e Vulcanologia, Osservatorio Vesuviano, Napoli, Italy
[e] Elettra-Sincrotrone Trieste S.C.p.A., Basovizza, Trieste, Italy
[f] School of Earth and Atmospheric Sciences, Georgia Institute of Technology, Atlanta, USA
[g] Institute of Petrology and Geochemistry, ETH, Zurich, Switzerland

ARTICLE INFO

Article history:
Received 10 July 2013
Accepted 24 December 2013
Available online 2 January 2014

Keywords:
Explosive eruptions
Campi Flegrei
Permeability
Viscosity

ABSTRACT

In order to understand outgassing during volcanic eruptions, we performed permeability measurements on trachy-phonolitic pyroclastic products from the Campanian Ignimbrite and Monte Nuovo, two explosive eruptions from the active Campi Flegrei caldera, Southern Italy. Viscous (Darcian) permeability spans a wide range between 1.22×10^{-14} and 9.31×10^{-11} m^2. Inertial (non-Darcian) permeability follows the same trend as viscous permeability: it increases as viscous permeability increases, highlighting the strong direct correlation between these two parameters. We observe that vesicularity does not exert a first order control on permeability: the Monte Nuovo scoria clasts are the most permeable samples but not the most vesicular; pumice clasts from the Campanian Ignimbrite proximal facies, whose vesicularity is comparable with that of Monte Nuovo scoriae, are instead the least permeable. In addition, we find that sample geometry exhibits permeability anisotropy as samples oriented parallel to vesicle elongation are more permeable than those oriented perpendicular. We compare our results with permeability values of volcanic products from effusive and explosive activity, and discuss the role of melt viscosity and crystallinity on magma permeability.

1. Introduction

Knowledge of permeability is of paramount importance for understanding the evolution of magma degassing during pre-, syn- and post-eruptive volcanic processes (Klug and Cashman, 1996; Rust and Cashman, 2004). Permeability results from the combination of various conduit processes related to magma vesiculation and crystallization that accompany magma rise from chamber/dykes along the conduit to the surface and/or to the formation of fractures due to shear fragmentation (Gonnermann and Manga, 2003; Tuffen and Dingwell, 2005). It is a key parameter in the transition from effusive to explosive volcanism (Eichelberger et al., 1986; Jaupart and Allegre, 1991; Woods and Koyaguchi, 1994; Kozono and Koyaguchi, 2009a,b; Degruyter et al., 2012), for example in the catastrophic failure from dome-forming eruptions to Vulcanian/Plinian behaviour (Lipman and Mullineaux, 1981; Herd et al., 2005). Permeability is also responsible for the quiescent gas loss from persistently degassing volcanoes (Oppenheimer et al., 2003), through formation of networks of continuously connected vesicles (Polacci et al., 2008), where gas percolates and can exit the volcanic system non-explosively (Burton et al., 2007). Quantifying permeability is therefore important for assessing the contribution of magmatic gases to the atmospheric global volatile budget (Gerlach, 2011).

Most permeability estimates existing to date refer to magmas of calc-alkaline compositions. Permeability measurements have been performed on pyroclastic products from andesitic to rhyolitic explosive eruptions (Klug and Cashman, 1996; Klug et al., 2002; Bernard et al., 2007; Bouvet de Maisonneuve et al., 2009; Wright et al., 2009; Degruyter et al., 2010a,b), on dome samples (Melnik and Sparks, 2002; Rust and Cashman, 2004; Mueller et al., 2005), and also on basaltic lavas and scoriae from effusive and mildly explosive volcanic activity (Saar and Manga, 1999; Mueller et al., 2005; Polacci et al., 2012). Permeability has also been measured in synthetic products from degassing experiments of volcanic material (Takeuchi et al., 2008; Bai et al., 2010, 2011). Mueller et al. (2005, 2008) compiled a thorough dataset that includes the only permeability values measured on trachytic volcanic rocks from a past sub-Plinian event: the Agnano Monte Spina (AMS) eruption (4.1 ka, de Vita et al., 1999) from Campi Flegrei (CF), an active, hazardous caldera west of the city of Naples, Southern Italy (Fig. 1). In summary, these studies have illustrated that permeability is overall a function of vesicularity; yet abundant scattering in the permeability-vs.-vesicularity data from the previous works implies that permeability

* Corresponding author at: via della Faggiola 32, 56126 Pisa, Italy. Tel.: +39 0508311957; fax: +39 0508311942.
E-mail address: polacci@pi.ingv.it (M. Polacci).

0377-0273/$ – see front matter © 2014 Elsevier B.V. All rights reserved.
http://dx.doi.org/10.1016/j.jvolgeores.2013.12.002

Fig. 1. Google map of Campi Flegrei eruption outcrops and Neapolitan area with Campi Flegrei caldera on the west and Somma-Vesuvius on the east. Yellow dots indicate outcrops: 1 = Mondragone, 2 = San Nicola La Strada, 3 = Monte Nuovo, 4 = Monte di Procida.

depends also on other parameters of which the most important are vesicle size and throat size, vesicle shape and tortuosity (Wright et al., 2009; Degruyter et al., 2010a; Polacci et al., 2012).

Here we report the first permeability measurements performed on trachy-phonolitic pyroclastic products from the Campanian Ignimbrite (CI) and Monte Nuovo (MTN) eruptions, two explosive eruptions from CF that have very similar compositions but strongly differ in intensity, magnitude and eruption dynamics (Piochi et al., 2008 and references therein). The obtained results significantly enlarge the existing limited database on the permeability of CF magmas providing an important contribution to understanding and modelling degassing and eruptive processes at this highly risky volcanic caldera.

2. Samples and summary of main textural features

We have chosen to study the permeability of CI and MTN products for many reasons. First, the two eruptions represent the two end-embers (Plinian and Vulcanian, respectively) in the eruption intensity/magnitude spectrum typical of CF eruptions. Second, CI is the largest magnitude explosive event of the Mediterranean region in late Quaternary (dating 39 ka, De Vivo et al., 2001), while MTN is the last eruption that occurred in the caldera in A.D. 1538 (Di Vito et al., 1987). Finally, there exists in the literature a lot of information on these eruptions about their stratigraphy, deposit characteristics, eruption dynamics, compositional, geochemical and textural data that allows us to interpret the results of this study in a robust scientific context (Rosi et al., 1996; Civetta et al., 1997; Rosi et al., 1999; Polacci et al., 2003; D'Oriano et al., 2005; Piochi et al., 2005; Pappalardo et al., 2007; Piochi et al., 2008, and references therein).

The samples used in this study and the outcrop locations where they were collected are listed in Table 1 and Figs. 1 and 2. The CI sample suite includes pumice products from both distal pyroclastic flow (CI pf Sn and CI pf Mo, Table 1) and proximal breccia (CI BM MP, Table 1) facies, the former collected at San Nicola La Strada and Mondragone, the latter at Monte di Procida (Fig. 1). The MTN samples are pumice and scoria products belonging, respectively, to the lower (LMN) and upper (UM1 and UM2) stratigraphic sequence of the MTN cone (Table 1) and were collected at Monte Nuovo Oasi Park (Fig. 1). All samples from the same location/outcrop were collected approximately at the same stratigraphic height.

The CI distal pyroclastic flow pumice clasts are poorly porphyritic to aphyric (phenocryst content between <10 vol% and <3 vol%, Civetta et al., 1997; Pappalardo et al., 2007), highly vesicular (connected vesicularity ~71–89 vol%, Table 1) volcanic rocks with a mostly microlite-free (microlite content <2 vol%, Civetta et al., 1997; Pappalardo et al., 2007) glassy groundmass. They have foamy vesicle textures consisting of mostly spherical to sub-spherical to slightly deformed vesicles with micron-size walls around larger, interconnected vesicles (Fig. 2a). The CI pumice samples from the Breccia Museo proximal facies are phorphyritic (phenocryst content up to 15 vol%, Melluso et al., 1995), vesicular to highly vesicular (connected vesicularity ~52–73 vol%, Table 1) rocks consisting of a fine vesicle structure in a mostly microlite-free (microlite content <2 vol%, Melluso et al., 1995) glassy groundmass, and of large, interconnected sub-spherical vesicles around single crystals or crystal aggregates (Fig. 2b). The MTN scoria and pumice clasts are characterized by a microlite-bearing (crystal content between 25–32 vol%, D'Oriano et al., 2005; Piochi et al., 2008) groundmass with tabular, acicular, and dendritic alkali-feldpar microlites, as well as widespread magnetite microlites in the microlite-richer scoriae (Fig. 2c). Connected vesicularity ranges between 48 and 62 vol% (Table 1), and vesicles have very irregular shapes being deformed by the ubiquitous microlites. Large, irregularly-shaped, interconnected microcrack-like vesicles are very common in the scoria samples (Fig. 2c) (Piochi et al., 2008).

3. Permeability measurements

Connected vesicularity (the ratio between the volume of connected vesicles and the core bulk volume) and permeability measurements were performed on nineteen samples, 11 from the CI pyroclastic flow and breccia facies and 8 from the MTN cone deposits (Table 1). All samples were drilled into cores of about 2.5 cm in diameter and between 1.6 and 3.6 cm in height; their external volume was measured via water displacement for more precision (for a description of the procedure refer to Bouvet de Maisonneuve et al., 2009). Samples where vesicle elongation was clearly recognizable were drilled both parallel and perpendicular to that direction. In Table 1 they are reported as _Para and _Perp, respectively. Connected vesicularity was obtained by quantifying the volume of the core without connected vesicles (volume of glass + crystals + isolated vesicles) with a Quantachrome He-stereopycnometer, then subtracting it from, and dividing it by, the external volume of the core.

Permeability was measured on the same samples used for connected vesicularity measurements with a Porous Material Inc gas permeameter at the University of Geneva (Switzerland). The samples were inserted in a cylindrical chamber lined with rubber; such rubber was subsequently pushed towards the sample by air coming from the chamber sides to make the sample air-tight. Gas (air) was injected into the permeameter from the base of the chamber at increasing pressure and flow rate. The relative error of $\log(k_1)$ and $\log(k_2)$ in Figs. 3 and 4 was estimated to ~2% from multiple measurements of the same sample. To take into account energy loss due to both viscous and inertial effects, the one-dimensional form of the Forchheimer equation (Ruth and Ma, 1992; Rust and Cashman, 2004) was fit to our experimental data to obtain the viscous (Darcian) k_1 and inertial (non-Darcian) k_2 permeabilities:

$$\frac{P_i^2 - P_o^2}{2PL} = \frac{\mu}{k_1} v + \frac{\rho}{k_2} v^2 \quad (1)$$

where P_i (Pa) and P_o (Pa) are the high and low pressure on each side of a sample of length L, P (Pa) is the gas pressure at which the gas flow is measured, μ (Pa s) is the gas viscosity, ρ (kg/m^3) is the gas density

Table 1
Permeability measurements of the investigated Campi Flegrei pyroclastic products.

[a]Sample	Diameter (cm)	Height (cm)	Weight (g)	[b]VesC (%)	k_1 (m^2)	k_2 (m)
CI pf Sn 2bD	2.51	2.96	9.25	71.30	2.63E−11	1.85E−07
CI pf Sn 2bE	2.51	2.80	6.71	80.99	2.20E−12	1.52E−08
CI pf Sn 2bF	2.51	2.29	4.09	88.97	1.94E−12	2.01E−08
CI pf Mo 1bA	2.51	2.05	4.44	82.87	1.37E−11	5.23E−08
CI pf Mo 1bB	2.52	2.73	9.37	79.56	2.30E−12	1.94E−08
CI BM MP 1A_Para	2.50	3.23	6.11	72.72	2.58E−12	4.41E−08
CI BM MP 1A_Perp	2.50	3.61	10.97	64.92	1.39E−13	8.92E−10
CI BM MP 1B	2.50	2.71	9.45	57.86	1.07E−13	4.90E−10
CI BM MP 1C	2.51	3.01	12.14	54.51	5.05E−12	4.95E−08
CI BM MP 1E	2.51	3.11	11.86	56.32	4.85E−14	1.94E−10
CI BM MP 1F_Para	2.51	2.37	8.24	51.93	8.63E−13	1.06E−08
CI BM MP 1F_Perp	2.50	2.90	10.59	52.46	1.22E−14	4.78E−10
CI BM MP 1H_Para	2.51	3.35	10.62	62.80	3.60E−12	2.35E−08
MTN UM1 MN4top 4A	2.53	1.61	nd	nd	8.37E−11	7.30E−06
MTN UM1 MN4top 4B	2.52	2.95	18.05	56.70	9.31E−11	4.17E−06
MTN UM1 MN4top 5	2.53	2.95	18.43	55.85	8.28E−11	3.66E−06
MTN UM1 MN4top 7	2.74	2.97	19.12	62.10	2.27E−11	1.29E−06
MTN UM2 MN4inf 001_1A	2.49	2.95	19.78	50.60	6.82E−11	2.00E−06
MTN UM2 MN4inf 001_1B	2.69	3.08	19.78	59.35	4.05E−11	2.49E−06
MTN UM2 MN4inf 002_1A	2.53	1.86	12.54	52.63	1.57E−11	1.43E−06
MTN UM2 MN4inf 002_1B	2.51	3.00	19.75	51.93	1.78E−11	2.30E−06
MTN LM MN2 c3	2.50	3.05	21.27	48.12	2.85E−12	1.68E−07

nd stays for not determined.
[a] pf and BM stay for pyroclastic flows and Breccia Museo, respectively. In CI pf and CI BM sample labels indicate sample deposit location (Sn = San Nicola, Mo = Mondragone, MP = -Monte di Procida) and sample index; in MTN sample labels indicate the deposit stratigraphic unit (Upper member (UM1, UM2) or Lower member (LM)) and sample index.
[b] VesC stays for connected vesicularity.

and v (m/s) is the gas filter velocity (which is the volumetric flow rate per total cross-sectional area of the sample orthogonal to fluid flow), taken at atmospheric conditions. The first and second terms on the right of the equation represent the contribution of the viscous friction and that of inertia and turbulence, respectively.

4. Results

Viscous permeability (k_1) of the investigated samples spans a wide range of values between 1.22×10^{-14} to 9.31×10^{-11} m^2 (Table 1, Fig. 3a). We observe that the most permeable samples ($k_1 = 1.57 \times 10^{-11}$–$9.31 \times 10^{-11}$ m^2) are the scoria clasts from the upper units of MTN (Table 1); pumice samples from the proximal breccia facies of CI are instead the least permeable ($k_1 = 4.85 \times 10^{-14}$–$5.05 \times 10^{-12}$ m^2, Table 1). Pumice clasts from CI distal pyroclastic flows have intermediate permeabilities overlapping with both those of the former and the latter. Inertial permeability (k_2) follows the same trend as viscous permeability: it increases as viscous permeability increases (Table 1, Fig. 3b), highlighting the direct correlation between these two parameters that can be nicely fitted by a power-law relationship, $k_1 = 8.6 \times 10^{-7}\ k_2^{0.75}$ (Fig. 3c). We note that, in oriented samples, k_1 and k_2 are, respectively, at least 1 order and 2 orders of magnitude higher in samples oriented parallel to vesicle elongation (Table 1, Fig. 3a, b).

5. Discussion and conclusions

5.1. Comparison with permeability data of other silicic eruptions

CI and MTN permeability data compare well with data obtained from andesitic to the most evolved calc-alkaline volcanic rocks (10^{-15}–10^{-10} m^2, for references see Introduction). Comparisons between our measured CF permeabilities with permeability data measured in rhyolitic (frothy and tube parallel to vesicle elongation) pumices from the Kos Plateau Tuff (KPT) (Bouvet de Maisonneuve et al., 2009, and references therein), basaltic scoria from Ambrym volcano, Vanuatu Arc

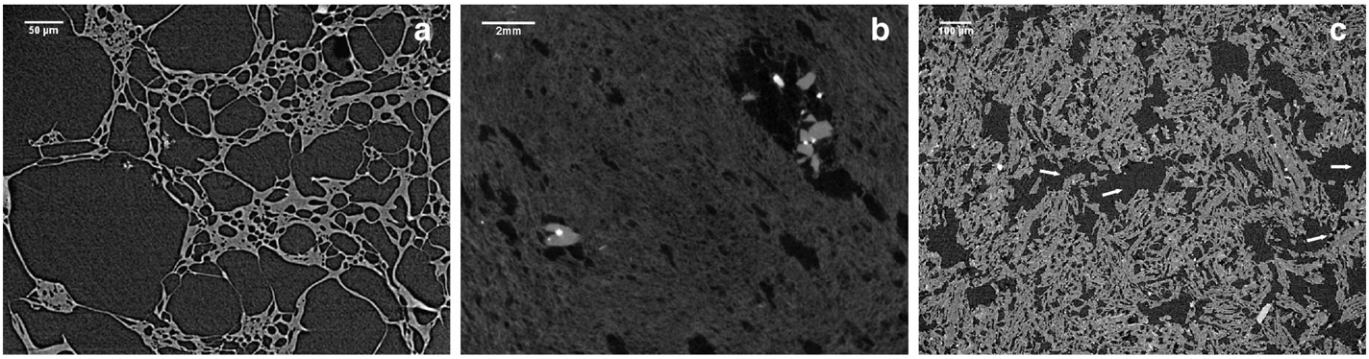

Fig. 2. Microtomographic axial slices of the Campi Flegrei samples used in this study: a) CI pyroclastic flow (CI pf, Sn + Mo) pumice, b) CI proximal (CI BM) breccia pumice, C) Monte Nuovo (MTN UM) scoria. Dark voids are vesicles, feldspar microphenocrysts are dark grey objects and oxides are bright spots; background groundmass is light grey. In (c) arrows indicate vesicle channels.

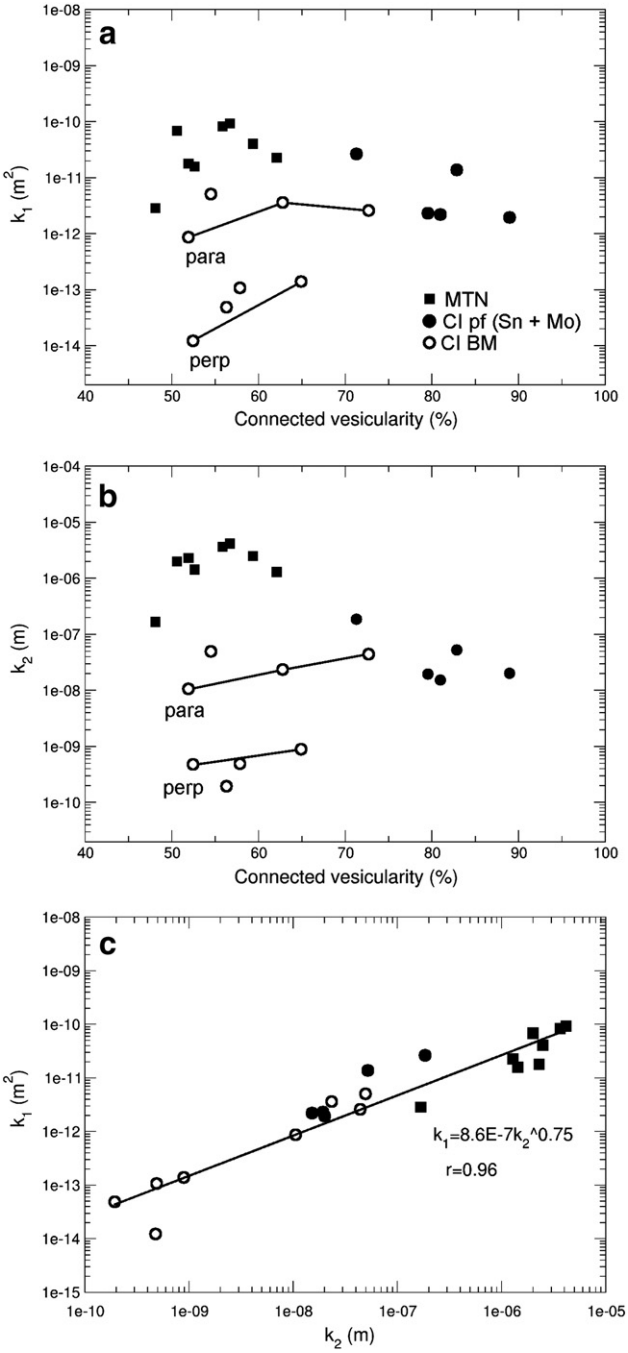

Fig. 3. Viscous k_1 (a) and inertial k_2 (b) permeability of the studied Campi Flegrei samples vs. connected vesicularity, and k_1 vs. k_2 (c). In these plots, closed and open circles indicate Cl distal pyroclastic flow (Cl pf, Sn + Mo) and proximal (Cl BM) breccia pumices, respectively. Closed squares indicate Monte Nuovo (MTN UM) samples. In (a) and (b) lines indicate samples cut parallel and perpendicular to vesicle elongation.

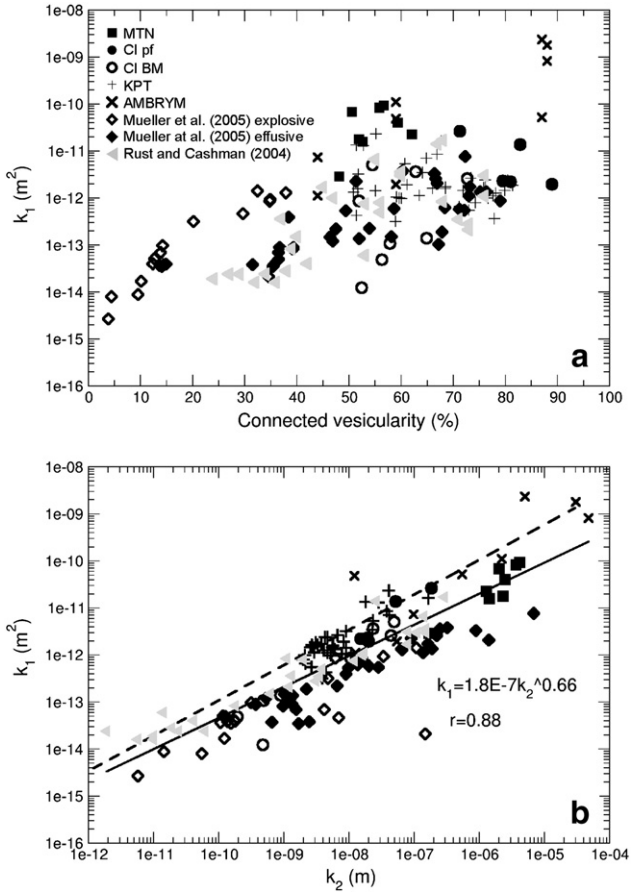

Fig. 4. Permeability (a) and k_1 vs. k_2 (b) of Campi Flegrei pyroclasts (same symbols as in Fig. 3), Kos Plateau Tuff (KPT) frothy and tube rhyolitic pumices (crosses), Ambrym basaltic scoria clasts (x), effusive (open diamonds) and explosive (full diamonds) products from Mueller et al. (2005), and obsidian flow samples from Rust and Cashman (2004). Dashed line is parameterization from Degruyter et al. (2012). See text for further explanation.

(Polacci et al., 2012), effusive and explosive volcanic products from Mueller et al. (2005), fallout pumice clasts from Little Glass Mountain (LGM), and obsidian flow samples from Little Glass Mountain (LGM) and Big Glass Mountain (BGM) (Rust and Cashman, 2004), are used to frame our results in a more global perspective (Fig. 4a, b). KPT frothy and tube pumices parallel to vesicle elongation plot in the same permeability–vesicularity field as Cl proximal breccia and distal pyroclastic flow products; their permeabilities partially overlap with, or are lower than, those measured in MTN scoria clasts, which are the highest amongst these compositionally evolved products. Basalt permeabilities are overall the highest and overlap with MTN data at connected vesicularities <60 vol%. Samples from Mueller et al. (2005) and Rust and Cashman (2004) mostly overlap with the plotted data and extend the dataset to the lowest end of the permeability vs. connected vesicularity range. Viscous and inertial permeabilities of all plotted samples are strongly correlated (Fig. 4b), and follow a power law relationship, $k_1 = 1.8 \times 10^{-7}\ k_2^{0.66}$ confirming, as highlighted in Fig. 3c, that the onset of inertial effects in the investigated samples is roughly the same independently of their composition (see discussion at Section 5.3).

5.2. Insights into conduit degassing

Similarly to mafic (Saar and Manga, 1999; Mueller et al., 2005, 2008; Polacci et al., 2012) and felsic (Klug and Cashman, 1996; Klug et al., 2002; Mueller et al., 2005, 2008; Bouvet de Maisonneuve et al., 2009; Wright et al., 2009) calc-alkaline natural magmas, we note that in evolved alkaline magmas i) vesicularity does not exert a first order control on permeability (e.g., the MTN samples are the most permeable but not the most porous), and that ii) sample geometry exhibits permeability anisotropy (Cl BM sample cores parallel to vesicle elongation display a higher permeability than perpendicular cores) (Wright et al., 2006). Assuming that the direction of elongated vesicles in the conduit works as a proxy for that of magma rising along the conduit to the surface, we suggest that magma degassing is stronger vertically than laterally in the conduit. Previous studies have indicated that the region where degassing vesicle pathways are most likely to occur is near and/or at the conduit walls (Cashman et al., 2000; Llewellin et al., 2002; Polacci et al., 2003; Bouvet de Maisonneuve et al., 2009; Caricchi et al.,

2011; Okumura et al., 2013), where the shear strain rate is maximum and magma viscosity becomes lower during magma rise due to viscous dissipation effects (Polacci et al., 2001; Rosi et al., 2004). These two conditions promote efficient vesicle coalescence and vesicle deformation to form a continuous pathway for gas to flow out of the system quiescently in both silicic (Okumura et al., 2009) and mafic (Burton et al., 2007) magmas. The centre and the region between the centre and conduit walls are also affected by magma degassing, although to a potentially minor extent, which recent experimental studies on rhyolitic obsidian have indicated as the mandatory requirement to trigger explosivity during a volcanic eruption (Okumura et al., 2013).

5.3. Insights into inertial effects in vesicular magmas

Quantifying inertial effects inside magmatic foams during outgassing is important for the transition from effusive to explosive eruptions. In the case inertial effects become dominant, explosive eruptions become more likely (Degruyter et al., 2012). From the permeability measurements we can obtain some insight into the onset of inertial effects inside magmatic foams during outgassing. The Forchheimer number (Fo), which is essentially a Reynolds number at the scale of the porous medium, provides an easy way to quantify this (Ruth and Ma, 1992). It is obtained from the quantities defined in Eq. (1),

$$Fo = \frac{\rho v k_1}{\mu k_2} \tag{2}$$

During volcanic eruptions the gas and magma phase are driven by the local pressure gradient across the conduit, which creates a difference in their velocity (Kozono and Koyaguchi, 2009a,b; Degruyter et al., 2012). This velocity difference creates an internal friction F_{mg} (Pa/m) between the two phases, which transfers momentum from the gas to the magma phase. The magnitude of this friction is quantified by the right hand side of the Forchheimer Eq. (1) where

$$v = v_g - v_m \tag{3}$$

and v_g (m/s) is the gas velocity and v_m (m/s) the magma velocity. If k_1 and k_2 are large enough, i.e. the permeability is high and the inertial effects are low, this internal friction will be small and the gas and magma will be able to flow at two separate velocities resulting into an effusive eruption. In the case where k_1 and k_2 are small the gas will transfer its momentum to the magma phase such that the two phases remain coupled and an explosive eruption occurs. When Fo becomes larger than 1, gas transport will be governed by the inertial term in the Forchheimer equation (second term in Eq. (1)). Inertia thus becomes dominant when the difference in gas and magma velocity exceeds a critical value,

$$v_g - v_m > \frac{\mu k_2}{\rho k_1} \tag{4}$$

As the gas density and viscosity will be mostly similar during outgassing in volcanic eruptions, the ratio k_1/k_2 will govern the onset of inertia for a given gas volume flux (Rust and Cashman, 2004). The results of this study fall in line with previous measurements of k_1 and k_2 (Fig. 4b; Rust and Cashman, 2004; Mueller et al., 2005; Takeuchi et al., 2008; Bouvet de Maisonneuve et al., 2009; Yokoyama and Takeuchi, 2009; Bai et al., 2010). A correlation between k_1 and k_2 exists, which can be fitted by a power law (Fig. 4b; Rust and Cashman, 2004). The correlation found between k_1 and k_2 can be reproduced by a simplified parameterization of these quantities proposed by Degruyter et al. (2012),

$$r_b = \left(\frac{\phi}{4/3\pi Nd(1-\phi)}\right)^{1/3} \tag{5}$$

$$k_1 = \frac{(f_{tb} r_b)^2}{8} \phi^m \tag{6}$$

$$k_2 = \frac{(f_{tb} r_b)}{f_0} \phi^{(1+3m)/2} \tag{7}$$

with Φ the connected vesicularity, f_{tb} the throat/vesicle ratio, r_b (m) the vesicle radius, Nd (m^{-3}) the vesicle number density, m the tortuosity, and f_0 the friction coefficient. An example fitted by the power-law relationship $k_1 = 5.6 \times 10^{-6}\ k_2^{0.78}$ is shown by the dashed line in Fig. 4b for representative values $f_{tb} = 0.2$, $Nd = 1 \times 10^{12}$ m^{-3}, $m = 3$, $f_0 = 50$. The trend itself is explained by the dependence of the pore space on the same parameters. The spread around the trend line is due to differences in throat/vesicle ratio, tortuosity, vesicle number density and roughness or factor/friction coefficient across the different samples. Rust and Cashman (2004) found that for values of k_1/k_2 exceeding the critical value, inertia will be significant in conduit flow models. Degruyter et al. (2012) demonstrated that inertia affects the transition from effusive to explosive eruptions, and that such transition is controlled by the ratio of a characteristic k_2 and the conduit radius. A small value of this ratio results in explosive eruptions.

5.4. The role of viscosity on permeability

Our data show that magmas with the same composition have strikingly different connected vesicularity–permeability values (e.g. MTN and CI samples); however, strikingly different magmas exhibit very similar connected vesicularity–permeability values (e.g. CI and KPT samples). For this reason, we suggest that similarities in permeability data can be generated by a balance between melt viscosity and crystal content as these will have a strong control on vesicle size and throat size and tortuosity (Wright et al., 2009; Degruyter et al., 2010a; Polacci et al., 2012).

We test this hypothesis by calculating the effect of crystals and dissolved water content on the viscosity of the CI, MTN, KPT and Ambrym magmas following Giordano et al. (2010) (Fig. 5, Table 2). From Fig. 5 it clearly emerges that Ambrym basaltic scoriae have the lowest melt and bulk (melt + crystals) viscosity. We believe that the lower bulk viscosity of these basaltic products may allow the development of large, interconnected vesicles with large vesicle apertures

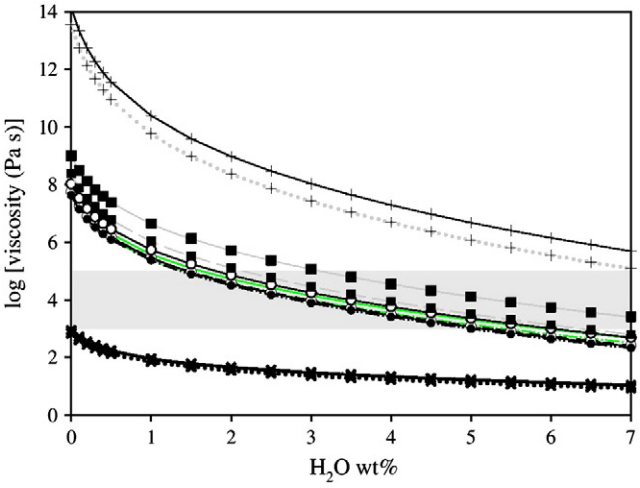

Fig. 5. Calculated water dependence for the viscosities of the CI distal pyroclastic flow pumices (CI pf, Sn + Mo), CI proximal (CI BM) breccia pumices, Monte Nuovo (MTN UM) scoria clasts, Kos Plateau Tuff (KPT) pumices and Ambrym scoria clasts reported in this study. Dashed/dotted and continuous curves refer, respectively, to the minimum and maximum viscosities calculated with the crystal content and temperature reported in Table 2. Symbols as in Fig. 3. See text for further details.

Table 2
Temperature, crystal content and relative viscosity of samples in Fig. 5.

Sample	T(°C)[a]	Crystal content[b] %		Min relative viscosity[c] (log unit)	Max relative viscosity[c] (log unit)
		Min	Max		
CI pf Sn	890	0	12	0.00	0.17
CI pf Mo	890	0	5	0.00	0.06
CI BM	890	0	17	0.00	0.27
MTN UM	890	25	35	0.33	0.94
KPT	700	25	35	0.33	0.94
Ambrym	1100	0	8	0.00	0.10

[a] eruptive T for CSn, ClMo, BM and MTN from Piochi et al. (2008); T for KPT from Bachmann, 2010; T for Ambrym from Allard et al. (2009).
[b] Crystal content of ClSn and ClMo from Civetta et al. (1997); for BM from Melluso et al. (1995); for MTN from Piochi et al., 2008; for KPT from Bouvet de Maisonneuve et al. (2009); for Ambrym from Polacci et al. (2012).
[c] in order to minimize and maximize relative viscosity, calculations were made following the procedure in Giordano et al. (2010) at strain-rates of 10^{-3} and 10^{-6} s^{-1}, respectively.

(Polacci et al., 2012) delivering the highest permeability values amongst the samples plotted in Fig. 4a. It also emerges that, although crystal content plays a non-negligible (up to a maximum of 0.6 log units) effect on the bulk viscosity of the samples illustrated in this study, water content could have an equally relevant effect (Fig. 5). In fact, although at the same water content the melt viscosity of KPT rhyolites is higher than that of MTN and CI trachytic melts, comparable values of calculated viscosity ($\log\eta$ (Pa s) $\simeq 4 +/- 1$; as these are calculations and not measurements they have an uncertainty of the order of 1 log unit) are obtained by assuming a dissolved water content of 7 wt.% for the KPT magma (Bachmann, 2010) ($\log\eta$ (Pa s) $\simeq 5$), 3 wt.% for the MTN magma (Piochi et al., 2008) ($\log\eta$ (Pa s) $\simeq 5$), 4 wt.% for the CI magma (Piochi et al., 2008) ($\log\eta$ (Pa s) $\simeq 3.5$), and very low water content for the Ambrym magma (Allard et al., 2009) ($\log\eta$ (Pa s) $\simeq 3$). In this view, we suggest that the high permeabilities of the MTN samples could be generated by a combination of high magnetite microlite content (Fig. 2c, Table 2) and the effect of dissolved volatiles on melt viscosity (Fig. 5). The effect of microlites is to promote both vesicle nucleation and growth on and around them, eventually enabling vesicles to coalesce and form a network of microcrack-like, permeable gas pathways (Piochi et al., 2008). CI pumice samples have permeabilities that are similar to those of KPT pumice products (Fig. 4a). While the former are essentially aphyric, their melt viscosity being still low enough (Fig. 5) to allow a high degree of vesicle coalescence and to form interconnected vesicle pathways (Fig. 2a, b), the latter displays the highest melt and bulk viscosity (Fig. 5). We propose here that crystallinity of the KPT magma was sufficiently high to counter balance the viscosity effect and allow vesicle to grow, coalesce and form permeable vesicle pathways well visible in tube pumices (Bouvet de Maisonneuve et al., 2009; Degruyter et al., 2010a). This process of vesicle coalescence enhancement by high crystallinity has been modelled numerically (Huber et al., 2012) and it has been documented to occur in crystal-rich magma analogues (Belien et al., 2010); it is likely to play a fundamental role on the development of permeability in any crystal-rich magma (e.g., basaltic magmas such as Stromboli (Bai et al., 2011), or silicic mushes (Huber et al., 2012)). However, the occurrence of this process in crystal-rich natural magmas deserves further textural and experimental investigation.

The cases provided in this study are just preliminary examples of the role that viscosity may have on magma textures and permeability. However, in order to determine if a correlation between viscosity and permeability exists, accurate determination of both the original dissolved water (and other volatiles) content and melt viscosity is therefore necessary to establish the role played by rheology in controlling magma physical properties and, consequently, magma textural evolution. Future studies on this topic should be focussed on detailed investigations of magma textures and their evolution with time under different conditions of deformation and cooling.

Acknowledgments

We thank the sedimentology laboratory of Section des Sciences de la Terre, University of Geneva, for allowing the use of the gas permeameter. We also thank Federica Marone and Christoph Hintermueller from the TOMCAT beamline at SLS, and Don R. Baker, Daria Zandomeneghi and Marco Voltolini for their help during tomographic runs. Patrizia Pantani helped with figure graphics. The SYRMEP beamline at Elettra is acknowledged for supporting part of the research. We thank Editor J. Marti and an anonymous reviewer for their constructive reviews on the original manuscript.

References

Allard, P., et al., 2009. Ambrym basaltic volcano (Vanuatu Arc): volatile fluxes, magma degassing rate and chamber depth. EOS Trans. Am. Geophys. Union 90 (52) (Fall Meet. Suppl.).
Bachmann, O., 2010. The petrologic evolution and pre-eruptive conditions of the rhyolitic Kos Plateau Tuff (Aegean Arc). Cent. Eur. J. Geosci. 2, 270–305. http://dx.doi.org/10.2478/v10085-010-0009-4.
Bai, L., Baker, D.R., Hill, R.J., 2010. Permeability of vesicular Stromboli basaltic glass: lattice Boltzmann simulations and laboratory measurements. J. Geophys. Res. 115, B07201. http://dx.doi.org/10.1029/2009JB007047.
Bai, L., Baker, D.R., Polacci, M., Hill, R.J., 2011. In-situ degassing study on crystal-bearing Stromboli basaltic magmas: implications for Stromboli explosions. Geophys. Res. Lett. 38, L17309. http://dx.doi.org/10.1029/2011GL048540.
Belien, I.B., Cashman, K.V., Rempel, A.W., 2010. Gas accumulation in particle-rich suspensions and implications for bubble populations in crystal-rich magma. Earth Planet. Sci. Lett. 297, 133–140.
Bernard, M.-L., Zamora, M., Géraud, Y., Boudon, G., 2007. Transport properties of pyroclastic rocks from Montagne Pelée volcano (Martinique, Lesser Antilles). J. Geophys. Res. 112, B05205. http://dx.doi.org/10.1029/2006JB004385.
Bouvet de Maisonneuve, C., Bachmann, O., Burgisser, A., 2009. Characterization of juvenile pyroclasts from the Kos Plateau Tuff (Aegean Arc): insights into the eruptive dynamics of a large rhyolitic eruption. Bull. Volcanol. 71, 643–658.
Burton, M.R., Mader, H.M., Polacci, M., 2007. The role of gas percolation in quiescent degassing of persistently active volcanoes. Earth Planet. Sci. Lett. 264, 46–60. http://dx.doi.org/10.1016/j.epsl.2007.08.028.
Caricchi, L., Pommier, A., Pistone, M., Castro, J., Burgisser, A., Perugini, D., 2011. Strain-induced magma degassing: Insights from simple-shear experiments on bubble bearing melts. Bull. Volcanol. 73, 1245–1257. http://dx.doi.org/10.1007/s00445-011-0471-2.
Cashman, K.V., Sturtevant, B., Papale, P., Navon, O., 2000. Magmatic fragmentation. In: Houghton, B.F., Rymer, H., Stix, J., McNutt, S., Sigurdsson, H. (Eds.), Encyclopedia of Volcanoes. Academic Press, San Diego, pp. 419–430.
Civetta, L., Orsi, G., Pappalardo, L., Fisher, R.V., Heiken, G., Ort, M., 1997. Geochemical zoning, mingling, eruptive dynamics and depositional processes of the Campanian Ignimbrite, Campi Flegrei caldera, Italy. J. Volcanol. Geotherm. Res. 75, 183–219.
D'Oriano, C., Poggianti, E., Bertagnini, A., Cioni, R., Landi, P., Polacci, M., Rosi, M., 2005. Changes in eruptive style during the A.D. 1538 Monte Nuovo eruption (Phlegrean Fields, Italy): the role of syn-eruptive crystallization. Bull. Volcanol. 67, 601–621. http://dx.doi.org/10.1007/s00445-004-0397-z.
de Vita, S., et al., 1999. The Agnano-Monte Spina eruption (4100 years BP) in the restless Campi Flegrei caldera (Italy). J. Volcanol. Geotherm. Res. 91, 269–301.
De Vivo, B., Rolandi, G., Gans, P.B., Calvert, A., Bohrson, W.A., Spera, F.J., Belkin, H.E., 2001. New constraints on the pyroclastic eruptive history of the Campanian volcanic Plain (Italy). Mineral. Petrol. 73, 47–65.
Degruyter, W., Bachmann, O., Burgisser, A., 2010a. Controls on magma permeability in the volcanic conduit during the climactic phase of the Kos Plateau Tuff eruption (Aegean Arc). Bull. Volcanol. 72, 63–74. http://dx.doi.org/10.1007/s00445-009-0302-x.

Degruyter, W., Burgisser, A., Bachmann, O., Malaspinas, O., 2010b. Synchrotron X-ray microtomography and lattice Boltzmann simulations of gas flow through volcanic pumices. Geosphere 6, 470–481. http://dx.doi.org/10.1130/GES00555.1.

Degruyter, W., Bachmann, O., Burgisser, A., Manga, M., 2012. The effects of outgassing on the transition between effusive and explosive silicic eruptions. Earth Planet. Sci. Lett. 349–350, 161–170. http://dx.doi.org/10.1016/j.epsl.2012.06.056.

Di Vito, M., Lirer, L., Mastrolorenzo, G., Rolandi, G., 1987. The 1538 Monte Nuovo eruption (Campi Flegrei, Italy). Bull. Volcanol. 49, 608–615.

Eichelberger, J.C., Carrigan, C.R., Westrich, H.R., Price, R.H., 1986. Non-explosive silicic volcanism. Nature 323, 598–602.

Gerlach, T., 2011. Volcanic versus anthropogenic carbon dioxide. EOS 92, 201–203.

Giordano, D., Polacci, M., Papale, P., Caricchi, L., 2010. Rheological control on the dynamics of explosive activity in the 2000 summit eruption of Mt. Etna. Solid Earth 1, 61–69. http://dx.doi.org/10.5194/se-1-61-2010.

Gonnermann, H.M., Manga, M., 2003. Explosive volcanism may not be an inevitable consequence of magma fragmentation. Nature 426, 432–435.

Herd, R.A., Edmonds, M., Bass, V.B., 2005. Catastrophic lava dome failure at Soufrière Hills Volcano, Montserrat, 12–13 July 2003. J. Volcanol. Geotherm. Res. 148, 234–252. http://dx.doi.org/10.1016/j.jvolgeores.2005.05.003.

Huber, C., Bachmann, O., Vigneresse, J.-L., Dufek, J., Parmigiani, A., 2012. A physical model for metal extraction and transport in shallow magmatic systems. Geochem. Geophys. Geosyst. 13. http://dx.doi.org/10.1029/2012GC004042.

Jaupart, C., Allegre, C., 1991. Gas content, eruption rate and instabilities of eruption regime in silicic volcanoes. Earth Planet. Sci. Lett. 102, 413–429.

Klug, C., Cashman, K.V., 1996. Permeability development in vesiculating magma. Bull. Volcanol. 58, 87–100.

Klug, C., Cashman, K.V., Bacon, C.R., 2002. Structure and physical characteristics of pumice from the climactic eruption of Mount Mazama (Crater Lake), Oregon. Bull. Volcanol. 64, 486–501.

Kozono, T., Koyaguchi, T., 2009a. Effects of relative motion between gas and liquid on 1-dimensional steady flow in silicic volcanic conduits. 1. An analytical method. J. Volcanol. Geotherm. Res. 180, 21–36.

Kozono, T., Koyaguchi, T., 2009b. Effects of relative motion between gas and liquid on 1-dimensional steady flow in silicic volcanic conduits. 2. Origin of diversity of eruption styles. J. Volcanol. Geotherm. Res. 180, 37–49.

Lipman, P.W., Mullineaux, D.R., 1981. The 1980 eruptions of Mount St. Helens, Washington. USGS professional paper 1250. 844.

Llewellin, E.W., Mader, H.M., Wilson, S.D.R., 2002. The constitutive equation and flow dynamics of bubbly magmas. Geophys. Res. Lett. 29, 2170. http://dx.doi.org/10.1029/2002gl015697.

Melluso, L., Morra, Perrotta, A., Scarpati, C., Addabbo, M., 1995. The eruption of The Breccia Museo (Campi Flegrei, Italy): fractional crystallization processes in a shallow, zoned magma chamber and implications for the eruptive dynamics. J. Volcanol. Geotherm. Res. 68, 325–339.

Melnik, O., Sparks, R.S.J., 2002. Dynamics of magma ascent and lava extrusion at Soufriere Hills Volcano, Montserrat. In: Druitt, T., Kokelaar, B. (Eds.), The Eruption of Soufriere Hills Volcano, Montserrat, from 1995 to 1999. The Geological Society of London, pp. 153–171.

Mueller, S., Melnik, O., Spieler, O., Scheu, B., Dingwell, D.B., 2005. Permeability and degassing of dome lavas undergoing rapid decompression: an experimental determination. Bull. Volcanol. 67, 526–538. http://dx.doi.org/10.1007/s00445-004-0392-4.

Mueller, S., Scheu, B., Spieler, O., Dingwell, D.B., 2008. Geology 36, 399–402. http://dx.doi.org/10.1130/G24605A.1.

Okumura, S., Nakamura, M., Takeuchi, S., Tsuchiyama, A., Nakano, T., Uesugi, K., 2009. Magma deformation may induce non-explosive volcanism via degassing through bubble networks. Earth Planet. Sci. Lett. 281, 267–274.

Okumura, S., Nakamura, M., Uesugi, K., Nakano, T., Fujioka, T., 2013. Coupled effect of magma degassing and rheology on silicic volcanism. Earth Planet. Sci. Lett. 362, 163–170.

Oppenheimer, C., Pyle, D.M., Barclay, J., 2003. Volcanic degassing. Geol. Soc. Lond. Spec. Publ. 213, 420.

Pappalardo, L., Ottolini, L., Mastrolorenzo, G., 2007. The Campanian Ignimbrite (southern Italy) geochemical zoning: insight on the generation of a super-eruption from catastrophic differentiation and fast withdrawal. Contrib. Mineral. Petrol. http://dx.doi.org/10.1007/s00410-007-0270-0.

Piochi, M., Mastrolorenzo, G., Pappalardo, L., 2005. Magma ascent and eruptive processes from textural and compositional features of Monte Nuovo pyroclastic products, Campi Flegrei, Italy. Bull. Volcanol. 67, 663–678. http://dx.doi.org/10.1007/s00445-005-0410-1.

Piochi, M., Polacci, M., De Astis, G., Zanetti, A., Mangiacapra, A., Vannucci, R., Giordano, D., 2008. Texture and composition of pumices and scoriae from the Campi Flegrei caldera (Italy): implications on the dynamics of explosive eruptions. Geochem. Geophys. Geosyst. 9, Q03013. http://dx.doi.org/10.1029/2007GC001746.

Polacci, M., Papale, P., Rosi, M., 2001. Textural heterogeneities in pumices from the climactic eruption of Mount Pinatubo, 15 June 1991, and implications for magma ascent dynamics. Bull. Volcanol. 63, 83–97.

Polacci, M., Pioli, L., Rosi, M., 2003. The Plinian phase of the Campanian Ignimbrite eruption (Phlegrean Fields, Italy): evidence from density measurements and textural characterization of pumice. Bull. Volcanol. 65, 418–432. http://dx.doi.org/10.1007/s00445-002-0268-4.

Polacci, M., Baker, D.R., Bai, L., Mancini, L., 2008. Large vesicles record pathways of degassing at basaltic volcanoes. Bull. Volcanol. 70, 1023–1029. http://dx.doi.org/10.1007/s00445-007-0184-8.

Polacci, M., Baker, D.R., La Rue, A., Mancini, L., 2012. Degassing behaviour of vesiculated basaltic magmas: an example from Ambrym volcano, Vanuatu Arc, and comparison to Stromboli, Aeolian Islands, Italy. J. Volcanol. Geotherm. Res. 233–234, 55–64. http://dx.doi.org/10.1016/j.jvolgeores.2012.04.019.

Rosi, M., Vezzoli, L., Aleotti, P., De Censi, M., 1996. Interaction between caldera collapse and eruptive dynamics during the Campanian Ignimbrite eruption, Phlegrean Fields, Italy. Bull. Volcanol. 57, 541–554.

Rosi, M., Vezzoli, L., Castelmenzano, A., Grieco, G., 1999. Plinian pumice fall deposit of the Campanian Ignimbrite eruption (Phlegrean Fields, Italy). J. Volcanol. Geotherm. Res. 91, 179–198.

Rosi, M., Landi, P., Polacci, M., Di Muro, A., Zandomeneghi, D., 2004. Role of conduit shear on ascent of the crystal-rich magma feeding the 800-year B.P. Plinian eruption of Quilotoa volcano (Ecuador). Bull. Volcanol. 66, 307–321.

Rust, A.C., Cashman, K.V., 2004. Permeability of vesicular silicic magma: inertial and hysteresis effects. Earth Planet. Sci. Lett. 228, 93–107.

Ruth, D., Ma, H., 1992. On the derivation of the Forchheimer equation by means of the averaging theorem. Transp. Porous Media 7, 255–264.

Saar, M.O., Manga, M., 1999. Permeability-porosity relationship in vesicular basalts. Geophys. Res. Lett. 26, 111–114.

Takeuchi, S., Nakashima, S., Tomiya, A., 2008. Permeability measurements of natural and experimental volcanic materials with a simple permeameter: toward an understanding of magmatic degassing processes. J. Volcanol. Geotherm. Res. 177, 329–339.

Tuffen, H., Dingwell, D.B., 2005. Fault textures in volcanic conduits: evidence for seismic trigger mechanisms during silicic eruptions. Bull. Volcanol. 67, 370–387.

Woods, A.W., Koyaguchi, T., 1994. Transitions between explosive and effusive eruptions of silicic magmas. Nature 370, 641–644.

Wright, H.M.N., Roberts, J.J., Cashman, K.V., 2006. Permeability of anisotropic tube pumice: model calculations and measurements. Geophys. Res. Lett. 33, L17316. http://dx.doi.org/10.1029/2006GL027224.

Wright, H.M.N., Cashman, K.V., Gottesfeld, E.H., Roberts, J.J., 2009. Pore structure of volcanic clasts: measurements of permeability and electrical conductivity. Earth Planet. Sci. Lett. 280, 93–104.

Yokoyama, T., Takeuchi, S., 2009. Porosimetry of vesicular volcanic products by a water-expulsion method and the relationship of pore characteristics to permeability. J. Geophys. Res. 114, B02201. http://dx.doi.org/10.1029/2008JB005758.